Bifurcation and Chaotic Analysis for Cable Vibration of a Cable-stayed Bridge

F.B. Gao[1,2,*], R.F. Wang[1], and S.K. Lai[3,4]

[1] School of Mathematical Science, Yangzhou University, Yangzhou 225002, China

[2] Departament de Matemàtiques, Universitat Autònoma de Barcelona, Bellaterra 08193, Barcelona, Spain

[3] Department of Civil and Environmental Engineering, The Hong Kong Polytechnic University, Kowloon, Hong Kong, China

[4] Hong Kong Branch of National Rail Transit Electrification and Automation Engineering Technology Research Center, The Hong Kong Polytechnic University, Kowloon, Hong Kong, China

Abstract. Cable-stayed bridges are of the most unique and cost-effective designs in modern bridge engineering. A key feature of these structures is that the cables or stays run directly from the tower to the deck. The nonlinear dynamic behavior of these cables can significantly affect the resilience and safety of the bridge. In this context, a deeper understanding of the bifurcation and chaotic mechanisms of cable vibration is highly desirable. Accordingly, in this study the nonlinear dynamic equation of a planar cable is derived for quantitative and qualitative analysis. The nonlinear system is solved asymptotically, using the conventional perturbation and two-timing scale methods, to study the periodic motion of the cables. The obtained solutions are primarily affected by the control parameters and the initial conditions. The asymptotic solutions are also simulated numerically. It is found that the chaotic behavior of cables is greatly affected by the governing parameters, including the cable dimensions, vibration amplitude, damping effect, and excitation frequency. Finally, seven state variables of the nonlinear system are analyzed to investigate the occurrence of bifurcation.

Keywords: Bifurcation and chaos; Asymptotic solution; Two-timing scale method; Cable-stayed bridge

1. INTRODUCTION

Cable-stayed bridges are a popular type of long-span flexible structure, composed of pressure-bearing towers, tension cables, and bending beam structures. In recent years, there has been growing interest in developing cable-stayed bridges in modern bridge engineering, owing largely to their favorable mechanical and structural performance, i.e., strong spanning ability and good seismic resistance.

The dynamic behavior of suspended cables has been somewhat widely studied in the engineering literature. For the free vibration model of a uniformly suspended cable, Irvine and Caughey [1] found that the analysis of the symmetric in-plane modes largely depends on a parameter that considers the influence of cable geometry and elasticity. To explore the effects of basic geometric and elastic parameters, wave-type and modal solutions were proposed by Irvine and Griffin [2]. Based on the problem of finite-amplitude vibrations of elastic suspended cables, bifurcation and chaos phenomena were investigated via the analysis of the characteristics of steady-state irregular dynamics [3-4]. Berlioz and Lamarque [5] presented a non-linear model for the dynamics of an inclined cable, using one or two degrees-of-freedom for in-plane displacement., and performing an analysis with multi-scale methods and experimental methods. Wang and Rega [6] studied the effects of sag, mass and inertia force on the transient dynamics of suspended cables with moving mass. Luongo and Piccardo [7]

*Corresponding author. E-mail: gaofabao@sina.com (F.B. Gao)

performed a multi-scale perturbation analysis on the cable equations with aeroelastic instability and internal resonance conditions. They also studied the existence of limit cycles and bifurcations by analyzing the stability of the system. Roy [8] summarized three main aspects of building a cable-stayed bridge, i.e., mathematical and experimental factors, tension and compression, and design configurations. In addition, two major types of cable-stayed bridge, the parallel attachment design and the radial attachment design, were also presented.

Cables are highly susceptible to vibration caused by various external excitations, particularly as their span increases, due to their small mass, large flexibility and low structural damping. In certain conditions, the wind-rain-induced vibration of cables and the start-oscillation condition can cause critical damage to cable-stayed bridges. Consequently, Gu [9] investigated the characteristics of wind-rain–induced cable vibrations, and Larsen and Larose [10] discussed the most common types of dynamic wind-effects encountered by cable-stayed bridges.

Cable-stayed bridges are also sensitive to seismic effects, owing to the low damping and high flexibility of the cables. The collapse of cable-stayed bridges during earthquakes has the potential to cause tremendous loss of life and devastation of property. As a result, Caicedo et al. [11, 12] presented a benchmark structural control problem for cable-stayed bridges, and provided relevant assessment criteria for controlling cable-stayed bridges subjected to seismic loads. More recently, Pang [13] investigated the seismic performance of multi-pylon cable-stayed bridges and developed a method to derive seismic fragility curves using a shaking-table test. Furthermore, Kang et al. [14] proposed a novel nonlinear dynamic model for cable-stayed bridges, and studied the internal resonance between the cables and the deck.

In real-life engineering environments, large-amplitude cable vibrations in cable-stayed bridges are harmful, and can induce mechanical fatigue in the cables. To understand this phenomenon, Abdelghaffar and Khalifa [15] analyzed the dynamic behavior of cable-stayed bridges using one-element and multiple-element cable systems. Lilien and Costa [16] studied a cable vibration problem caused by parametric excitations, i.e., where the dynamic instability of the cables is due to a small periodic motion of girders and masts. Their results showed that parametric excitations are very likely to affect the instability of long-span cable-stayed bridges due to the presence of many low frequencies in the girders and cables. Qian et al. [17] investigated the effect of deck vibration on cables, and proposed a nonlinear dynamic equation for cable-stayed bridges undergoing deck vibration. They found that the vertical vibration of the bridge deck has a combined parametric and forced excitation effect on the cables when the angle of the cable is considered. Chen and Sun [18] investigated the periodic motion of a cable-damper system using the multi-harmonic balance method, and presented the response of the system under various excitation frequencies. Recently, Su et al. [19, 20] studied the nonlinear vibration of the in-plane cable-stayed bridge using the transfer matrix method and an experimental method, respectively. To obtain the optimal arrangement of the cables on a cable-stayed bridge, Nithesh et al. [21] performed a comparative study on semi-sector, harp, and sector cable arrangements, which considered the axial force, cable force, bending moment, shear force and displacement.

Based on existing research, the amplitude of rain-induced cable vibration is primarily related to the surface material, cable length, wind yaw angle, and cable inclination direction. In the present work, we thus investigate the influences of these factors on the nonlinear dynamic behavior of cables . This paper is organized as follows. Section 2 formulates the nonlinear dynamical equation of a planar cable. In Section 3, asymptotic solutions of the nonlinear system are obtained using the perturbation

method and the two-timing scale method. The solution curves are also plotted and analyzed. In Section 4, the bifurcation and chaotic motions of the nonlinear system are presented. Finally, concluding remarks are given in Section 5.

2. NONLINEAR DYNAMICAL EQUATION OF THE STAY CABLE

The nonlinear dynamical equation for the cables on a cable-stayed bridge can be found in Ref. [17]. For the purpose of this study, we will not consider the initial deflection and the out-of-plane motion. Using the classical vibration theory [22, 23], the dynamical equation of a cable in the *xy* plane (Figure 1) is given by Eq. (1):

$$\rho A\frac{\partial^2 w}{\partial t^2}-T\frac{\partial^2 w}{\partial x^2}+2\mu\frac{\partial w}{\partial t}=\frac{EA}{L}\left[D(t)\cos\gamma+\frac{1}{2}\int_0^L\left(\frac{\partial w}{\partial x}\right)^2 dx\right]\frac{\partial^2 w}{\partial x^2} \tag{1}$$

with the boundary conditions given by Eq. (2):

$$w(0,t)=0,\ w(L,t)=D(t)\sin\gamma \tag{2}$$

If only the first-order vibration mode is considered, then the solution of Eq. (1) can be expressed as:

$$w(x,t)=\frac{x}{L}D(t)\sin\gamma+y(t)\sin\frac{\pi x}{L} \tag{3}$$

Let $\widehat{w}=w/L$. Then, Eqs. (1)–(3) can be re-written as Eqs. (4)–(6):

$$\frac{\partial^2\widehat{w}}{\partial\tau^2}-\frac{T}{\rho AL^2\omega^2}\frac{\partial^2\widehat{w}}{\partial\eta^2}+\frac{2\mu}{\rho AL\omega}\frac{\partial\widehat{w}}{\partial t}=\frac{E}{\rho L^2\omega^2}\left[d\cos\tau\cos\gamma+\frac{1}{2}\int_0^1\left(\frac{\partial\widehat{w}}{\partial\eta}\right)^2 d\eta\right]\frac{\partial^2\widehat{w}}{\partial\eta^2} \tag{4}$$

$$\widehat{w}(0,\tau)=0,\ \widehat{w}(1,\tau)=d\cos\tau\sin\gamma \tag{5}$$

$$\widehat{w}(\eta,\tau)=\eta d\cos\tau\sin\gamma+y(\tau)\sin(\pi\eta) \tag{6}$$

By substituting Eq. (6) into Eq. (4), the nonlinear dynamical equation in the *y* direction becomes:

$$\frac{d^2y}{d\tau^2}+2\xi\frac{dy}{d\tau}+\left[\lambda^2+c^2\left(d\cos\tau\cos\gamma+\frac{1}{2}d^2\cos^2\tau\sin^2\gamma\right)\right]y(\tau)+\frac{\pi^2c^2}{4}y^3(\tau)-\frac{\eta d}{\sin(\pi\eta)}\sin\gamma(\cos\tau-2\xi\sin\tau)=0 \tag{7}$$

The parameters of Eq. (7) are given by the following definitions:

$$\xi=\frac{\mu}{\rho A\omega L},\ \lambda=\frac{\pi}{\omega L}\sqrt{\frac{T}{\rho A}}=\frac{\omega_0}{\omega},\ \omega_0=\frac{\pi}{L}\sqrt{\frac{T}{\rho A}},$$

$$c=\frac{\pi}{\omega L}\sqrt{\frac{E}{\rho}},\ d=\frac{D}{L},\ \eta=\frac{x}{L},\ \tau=\omega t$$

where μ is the damping of the cable system, ρ is the density, ω is the excitation frequency, L is the cable length, A is the cross-sectional area of the cable, $W=\rho A$ is the mass per unit length, T is the axial tensile force, E is the modulus of elasticity, γ is the angle between the cable and its vertical direction, and $D(t)=D\cos(\omega t)$, where D is the vibration amplitude of the anchorage point. Note that Eq. (7) differs from the dynamical model derived in Ref. [17].

Figure 1. Schematic diagram of a cable.

3. ASYMPTOTIC SOLUTIONS OF THE NONLINEAR SYSTEM

In this section, we derive asymptotic solutions for the system represented by Eq. (7). This system can be solved by using two perturbation-based approaches: the conventional perturbation method, and the two-timing scale method. The solutions

obtained using both of these methods are presented and discussed.

3.1 Perturbation method

Let the initial values of the system represented by Eq. (7) be represented by Eq. (8):

$$y(0) = a,\ y'(0) = b \tag{8}$$

Suppose that the asymptotic solution of Eq. (7) is expressed in terms of a small parameter ε $(0 < \varepsilon \ll 1)$ as defined by Eq. (9):

$$y(\tau) = \varepsilon y_1(\tau) + \varepsilon^2 y_2(\tau) + \varepsilon^3 y_3(\tau) + \cdots \tag{9}$$

Then, by substituting Eq. (9) into Eq. (7) and comparing the coefficients of powers of ε, we obtain Eq. (10):

$$\varepsilon^1: {y_1}'' + 2\xi {y_1}' + \left[\lambda^2 + c^2\left(d\cos\tau\cos\gamma + \frac{1}{2}d^2\cos^2\tau\sin^2\gamma\right)\right] y_1 = e_1\cos\tau + e_2\sin\tau \tag{10}$$

where $e_1 = \eta d\sin\gamma/\sin(\pi\eta)$ and $e_2 = -2\eta d\xi\sin\gamma/\sin(\pi\eta)$. Now, suppose that Eq. (10) has a solution of the form (Eq. (11)):

$$y_1(\tau) = a_0 + a_1\tau + a_2\tau^2 + a_3\tau^3 + \ldots \tag{11}$$

Then, substituting the Taylor series expansions for $\cos\tau$, $\cos^2\tau$ and $\sin\tau$ into Eq. (10), and comparing the coefficients of powers of τ, we obtain Eqs. (12) and (13):

$$\tau^0: 2a_2 + 2\xi a_1 + \left[\lambda^2 + c^2 d\left(\cos\gamma + \frac{1}{2}d\sin^2\gamma\right)\right] a_0 = e_1 \tag{12}$$

$$\tau^1: 6a_3 + 4\xi a_2 + \left[\lambda^2 + c^2 d\left(\cos\gamma + \frac{1}{2}d\sin^2\gamma\right)\right] a_1 = e_2 \tag{13}$$

Let us suppose that $a_0 = a_1 = 0$. Then it follows immediately that $a_2 = e_1/2$. Furthermore, substituting a_1 and a_2 into Eq. (13), we have $a_3 = (e_2 - 2e_1\xi)/6$. Similarly, we can obtain $a_4 = -e_2\xi/12 - e_1\left[\lambda^2 + c^2\left(d\cos\gamma + \frac{1}{2}d^2\sin^2\gamma\right) + 1 - 4\xi^2\right]/24$. We thus have Eq. (14):

$$y_1(\tau) = a_2\tau^2 + a_3\tau^3 + a_4\tau^4 + o(\tau^5) \tag{14}$$

with a_2, a_3 and a_4 as defined above.

Following the same procedure, we obtain Eqs. (15) and (16):

$$y_2 = b_1\tau + b_2\tau^2 + b_3\tau^3 + b_4\tau^4 \tag{15}$$

$$y_3 = c_1\tau + c_2\tau^2 + c_3\tau^3 + c_4\tau^4 + c_5\tau^5 + c_6\tau^6 + c_7\tau^7 + c_8\tau^8 \tag{16}$$

where the coefficients $b_i (i = 1 - 4)$ and $c_i (i = 1 - 8)$ are presented in the Appendix.

Finally, substituting Eqs. (14)–(16) into Eq. (9), it follows that the asymptotic solution of the system represented by Eq. (7) is given by Eq. (17):

$$y(\tau) = \varepsilon(a_2\tau^2 + a_3\tau^3 + a_4\tau^4) + \varepsilon^2(b_1\tau + b_2\tau^2 + b_3\tau^3 + b_4\tau^4) + \varepsilon^3(c_1\tau + c_2\tau^2 + c_3\tau^3 + c_4\tau^4 + c_5\tau^5 + c_6\tau^6 + c_7\tau^7 + c_8\tau^8) \tag{17}$$

3.2 Two-timing scale method

Consider the transformation (18):

$$\xi \to \varepsilon\mu,\ c^2 d\cos\gamma \to \varepsilon g_1,\ \frac{1}{2}c^2 d\sin^2\gamma \to \varepsilon^2 g_2,\ \frac{\pi^2 c^2}{4} \to \varepsilon^2 g_3 \tag{18}$$

Under this transformation, Eq. (7) becomes Eq. (19):

$$\frac{d^2y}{d\tau^2} + 2\varepsilon\mu\frac{dy}{d\tau} + (\lambda^2 + \varepsilon g_1\cos\tau + \varepsilon^2 g_2\cos^2\tau)y(\tau) + \varepsilon^2 g_3 y^3(\tau) = e_1\cos\tau - 2\varepsilon\mu e_1\sin\tau \tag{19}$$

To use the two-timing scale method, we assume that the first-order approximate solution of Eq. (19) is of the form below:

$$y(\varepsilon,t) = y_0(T_1,T_2) + \varepsilon y_1(T_1,T_2) \tag{20}$$

where $T_1 = \tau$ and $T_2 = \varepsilon\tau$ are fast and slow time scales, respectively.

Then, substituting Eq. (20) into Eq. (19) and comparing the coefficients of powers of ε, we derive Eqs. (21)–(23):

$$\varepsilon^0: \partial_{T_1T_1} y_0 + \lambda^2 y_0 = e_1 \cos T_0 \tag{21}$$

$$\varepsilon^1: \partial_{T_1T_1} y_1 + \lambda^2 y_1 = -2\partial_{T_1T_2} y_0 - 2\mu\partial_{T_0} y_0 - g_1 \cos T_0 y_0 - 2\mu e_1 \sin T_0 \tag{22}$$

$$\begin{aligned}\varepsilon^2: \partial_{T_1T_1} y_2 + \lambda^2 y_2 = &-\partial_{T_2T_2} y_0 - 2\partial_{T_1T_2} y_1 - 2\mu\left(\partial_{T_2} y_0 + \partial_{T_1} y_1\right) \\ &- g_1 \cos T_0 y_1 - g_2 \cos^2 T_0 y_0\end{aligned} \tag{23}$$

If we suppose that the solution of Eq. (21) is Eq. (24):

$$y_0 = A(T_2)e^{i\lambda T_1} + \bar{A}(T_2)e^{-i\lambda T_1} - \frac{e_1}{2(1-\lambda^2)}\left(e^{iT_1} + e^{-iT_1}\right) \tag{24}$$

Then, substituting Eq. (24) into Eq. (22) and eliminating the secular terms, we obtain:

$$A(T_2) = \bar{A}(T_2) = e^{-\mu T_2} \tag{25}$$

The same procedures also yield Eq. (26):

$$\begin{aligned} y_1 = &\frac{\mu e_1 \lambda^2}{(1-\lambda^2)^2}\left(e^{iT_1} - e^{-iT_1}\right) + \frac{g_1}{2}\left[\frac{e^{-\mu T_2}}{1+2\lambda}\left(e^{i(1+\lambda)T_1} + e^{-i(1+\lambda)T_1}\right)\right. \\ &\left. - \frac{e^{-\mu T_2}}{2\lambda-1}\left(e^{i(\lambda-1)T_1} + e^{-i(\lambda-1)T_1}\right) + \frac{e_1}{2(1-\lambda^2)(\lambda^2-4)}\left(e^{2iT_1} + e^{-2iT_1}\right) + \frac{e_1}{\lambda^2(1-\lambda^2)}\right] \\ &+ B(T_2)e^{i\lambda T_1} + \bar{B}(T_2)e^{-i\lambda T_1}\end{aligned} \tag{26}$$

where

$$B(T_2) = \bar{B}(T_2) = \frac{4\mu^2 - g_2}{4g_1 \cos T_1} e^{-\mu T_2}$$

We thus have Eqs. (27) and (28):

$$y_0 = 2e^{-\mu T_2}\cos(\lambda T_1) - \frac{e_1}{1-\lambda^2}\cos T_1, \tag{27}$$

$$\begin{aligned} y_1 = &\frac{2\mu e_1 \lambda^2 \sin T_1}{(1-\lambda^2)^2} + \frac{g_1}{2}\left(\frac{2e^{-\mu T_2}\cos(1+\lambda)T_1}{1+2\lambda} - \frac{2e^{-\mu T_2}\cos(\lambda-1)T_1}{2\lambda-1}\right. \\ &\left. + \frac{e_1 \cos 2T_1}{(1-\lambda^2)(\lambda^2-4)} + \frac{e_1}{\lambda^2(1-\lambda^2)}\right) + \frac{4\mu^2 - g_2}{2g_1 \cos T_0}\cos(\lambda T_1)\end{aligned} \tag{28}$$

It follows that the first-order approximate solution of Eq. (19) is:

$$\begin{aligned} y = &2e^{-\mu T_2}\cos(\lambda T_1) - \frac{e_1}{1-\lambda^2}\cos T_1 + \varepsilon\left\{\frac{2\mu e_1 \lambda^2 \sin T_1}{(1-\lambda^2)^2}\right. \\ &+ \frac{g_1}{2}\left[\frac{2e^{-\mu T_2}\cos(1+\lambda)T_1}{1+2\lambda} - \frac{2e^{-\mu T_2}\cos(\lambda-1)T_1}{2\lambda-1}\right. \\ &\left.\left. + \frac{e_1 \cos 2T_1}{(1-\lambda^2)(\lambda^2-4)} + \frac{e_1}{\lambda^2(1-\lambda^2)}\right] + \frac{4\mu^2 - g_2}{2g_1 \cos T_0}\cos(\lambda T_1)\right\}\end{aligned} \tag{29}$$

where $g_1 = c^2 d\cos\gamma$ and $g_2 = c^2 d\sin^2\gamma/2$.

3.3 Results and Discussion

To verify the effectiveness of both asymptotic approaches, we compute the solutions for the parameters listed in Table 1. The initial conditions of system (7) are taken as $a = -0.0002046$ and $b = 0$, and the parameter $\varepsilon = 0.01$. The solution curves obtained using the conventional perturbation method in Eq. (17), the two-timing scale method in Eq. (29), and direct numerical integration of the original system (7), are shown in Figure 2. The solution obtained using the conventional perturbation method is only valid for a very short period of time; as time increases, it deviates significantly from the numerical solution of the original equation (i.e., "exact solution"). In contrast, the solution

obtained using the two-timing scale method is much more effective for analyzing the dynamic response of the cable. Indeed, the results show that the asymptotic solution obtained using this method provides good agreement with the "exact solution" (Figures 2 and 3).

Table 1: The geometrical and material properties of a cable [17].

Figure 2. A comparison between the conventional perturbation method solution (black curve), the two-timing scale method solution (blue curve), and the "exact solution" (red curve).

Figure 3. A comparison between the two-timing scale method solution (blue curve), and the "exact solution" (red curve).

4. BIFURCATION ANALYSIS

4.1 Bifurcation and chaotic behavior of the system

In this section, we consider the effects of various parameters, including cable dimensions, material properties, vibration amplitude, inclination angle, damping effect, and excitation frequency, on the bifurcation and chaotic motion of the system given by Eq. (7). The initial conditions are taken as $a = 0.00001$ and $b = 0$, and the parameters are as listed in Table 1.

We first study the influence of the cross-sectional area of the cable (*A)* on the cable displacement in the *y*-direction (*y*). For this purpose, we consider the 3:1 parametric resonance condition. This refers to when the excitation frequency ω is three times the natural frequency of the system ω_0. The bifurcation diagram for the variation of the parameter *A* and the displacement *y* is shown in Figure 4. The results indicate that there are chaotic motions in the system as the cross-sectional area of the cable changes. When the cross-sectional area is less than 6 mm^2, the vibration amplitude of the cable is relatively large. As the cross-sectional area increases, the amplitude stabilizes.

Figure 4. Bifurcation diagram for the cross-sectional area of the cable (*A*) and the displacement (*y).*

We also consider the effect of the vibration amplitude of the anchorage point (*D*) on the cable displacement in the y-direction. The corresponding bifurcation diagram is shown in Figure 5. The diagram indicates that the cable exhibits both chaotic and periodic motions. In Figure 6, the phase portrait and time-domain curves for the system when $D = 0.0052101$ are presented.

We next analyze the effect of the inclination angle between the cable and its vertical direction (γ) on the cable displacement in the y-direction. The corresponding bifurcation diagram is presented in Figure 7. Meanwhile, in Figure 8, the phase portrait and time-domain curves when $\gamma = 1.1114$ are depicted.

We also investigate the impact of the cable length (*L)* on the cable displacement in the *y* direction. The corresponding bifurcation diagram is provided in Figure 9. The results demonstrate that there are chaotic motions in the system as the cable length varies.

Figure 5. Bifurcation diagram for the vibration amplitude of the anchorage point (*D)* and the displacement (*y).*

Figure 6. Phase portrait and time domain curves of the system for $D = 0.0052101$.

Figure 7. Bifurcation diagram for the inclination angle (γ) and the displacement (*y)*.

Figure 8. Phase portrait and time domain curves of the system for $\gamma = 1.1114$.

Figure 9. Bifurcation diagram for the cable length (*L)* and the displacement (*y)*.

We are also interested in the relationship between the damping effect (μ) and the cable displacement in the *y*-direction (*y*). The corresponding bifurcation diagram is shown in Figure 10. The results indicate that, while there are chaotic motions in the system as the damping value varies, the effect is not particularly strong for any value of the damping.

We next analyze the impact of the excitation frequency ω on the cable displacement in the *y*-direction. The corresponding bifurcation diagram is presented in Figure 11. The vibration amplitude of the system is observed to increase as the excitation frequency increases. Figure 12 provides the phase portrait and time-domain curves when $\omega = 42.8686$.

Finally, we consider the effect of the density of the cable (ρ) on the cable

displacement in the y direction (y). The corresponding bifurcation diagram is included in Figure 13. This diagram indicates that the influence of the density on the dynamic response of the cable is significant. As the value of ρ increases, the vibration amplitude of the system in the y direction is, to a certain extent, stable.

Figure 10. Bifurcation diagram for the damping effect (μ) and the displacement (y).
Figure 11. Bifurcation diagram for the excitation frequency (ω) and the displacement (y).
Figure 12. Phase portrait and time domain curves of the system for $\omega = 42.8686$.
Figure 13. Bifurcation diagram for the cable density (ρ) and the displacement (y).

4.2 Periodic motion

Two metrics, namely length and density, are critical factors in determining the periodic motion of the cable system. In this section, we further investigate the influence of these two parameters. Further numerical simulations, alongside those presented in Section 4.1, indicate that various kinds of periodic motion for the cable system are possible (Figures 14-19). The parameters for these simulations are once more listed in Table 1. Note that the initial conditions of the system are now also varied.

Figure 14. Phase portrait diagram for L = 11.4211 and $[a, b] = [0.0001, 0]$.
Figure 15. Phase portrait diagram for L = 11.4211 and $[a, b] = [-0.0001, 0]$.
Figure 16. Phase portrait diagram for L = 11.4211 and $[a, b] = [-0.0001, 0.00006]$.
Figure 17. Phase portrait diagram for L = 11.4211 and $[a, b] = [-0.002046, 0]$.
Figure 18. Phase portrait diagram for ρ = 0.0258 and $[a, b] = [-0.0001, 0.0001]$.
Figure 19. Phase portrait diagram for ρ = 0.0258 and $[a, b] = [0.001, 0.0004]$.

5. CONCLUSIONS

In this work, the nonlinear dynamic behavior of a planar cable is studied. To analyze the vibration mechanism, the asymptotic solutions of the nonlinear dynamical equation are obtained using the conventional perturbation and the two-timing scale methods. It is found that the solutions obtained using the conventional perturbation method are only valid for a very short period of time, while those obtained using the two-timing scale method correspond closely to the exact solutions. It is also observed that the nonlinear dynamic behavior of the cable system becomes complicated as the control parameters are varied, due to the existence of nonlinear terms. Consequently, the state variables of the system are considered for bifurcation analysis, as a function of seven parameters. The results indicate that as these parameters vary, the cable system can change from exhibiting periodic motion to chaotic motion. The effects of these parameters on various kinds of periodic motion displayed by the system are also presented and discussed.

ACKNOWLEDGMENTS

The authors gratefully acknowledge the support of the National Natural Science Foundation of China (NSFC) through Grant Nos. 11672259 and 11571301; the China Scholarship Council through Grant No.201908320086; and the Ministry of Land and Resources Research of China in the Public Interest through Grant No. 201411007. The funding support from the Research Impact Fund (Project No. R-5020-18) of the Research Grants Council of the Hong Kong Special Administrative Region is also gratefully acknowledged.

APPENDIX

$$b_1 = 1,$$

$$b_2 = -\xi,$$

$$b_3 = \frac{1}{6}\left\{4\xi^2 - \left[\lambda^2 + c^2\left(d\cos\gamma + \frac{1}{2}d^2\sin^2\gamma\right)\right]\right\},$$

$$b_4 = \frac{1}{6}\left[\lambda^2 + c^2\left(d\cos\gamma + \frac{1}{2}d^2\sin^2\gamma\right) - 2\xi\right]\xi,$$

$$c_1 = 1,$$

$$c_2 = -\xi,$$

$$c_3 = \frac{4\xi^2 - \left[\lambda^2 + c^2\left(d\cos\gamma + \frac{1}{2}d^2\sin^2\gamma\right)\right]}{6},$$

$$c_4 = \frac{\left[\lambda^2 + c^2\left(d\cos\gamma + \frac{1}{2}d^2\sin^2\gamma\right) - 2\xi\right]\xi}{6},$$

$$c_5 = \frac{\left\{4\xi - \left[\lambda^2 + c^2\left(d\cos\gamma + \frac{1}{2}d^2\sin^2\gamma\right)\right]\right\}^2 - 4\xi^2\left[\lambda^2 + c^2\left(d\cos\gamma + \frac{1}{2}d^2\sin^2\gamma\right)\right]}{120} + \frac{c^2(d\cos\gamma + d^2\sin^2\gamma)}{40},$$

$$c_6 = -\frac{\left\{4 - \left[\lambda^2 + c^2\left(d\cos\gamma + \frac{1}{2}d^2\sin^2\gamma\right)\right]\right\}\xi^3}{90} + \frac{\left[\lambda^2 + c^2\left(d\cos\gamma + \frac{1}{2}d^2\sin^2\gamma\right)\right]\xi^2}{30} - \frac{\left[\lambda^2 + c^2\left(d\cos\gamma + \frac{1}{2}d^2\sin^2\gamma\right)\right]^2\xi}{120} - \frac{c^2(d\cos\gamma + d^2\sin^2\gamma)\xi}{40},$$

$$c_7 = \frac{\left\{4 - \left[\lambda^2 + c^2\left(d\cos\gamma + \frac{1}{2}d^2\sin^2\gamma\right)\right]\right\}\xi^4}{315} - \frac{\left[\lambda^2 + c^2\left(d\cos\gamma + \frac{1}{2}d^2\sin^2\gamma\right)\right]\xi^3}{105} + \frac{\left[\lambda^2 + c^2\left(d\cos\gamma + \frac{1}{2}d^2\sin^2\gamma\right) - 1\right]\left[\lambda^2 + c^2\left(d\cos\gamma + \frac{1}{2}d^2\sin^2\gamma\right)\right]\xi^2}{315} + \frac{19c^2(d\cos\gamma + d^2\sin^2\gamma)\xi^2}{1260} + \frac{\left[\lambda^2 + c^2\left(d\cos\gamma + \frac{1}{2}d^2\sin^2\gamma\right)\right]^2\xi}{630} + \frac{c^2(d\cos\gamma + d^2\sin^2\gamma)\left[\lambda^2 + c^2\left(d\cos\gamma + \frac{1}{2}d^2\sin^2\gamma\right)\right]}{720} - \frac{[c^2(d\cos\gamma + 4d^2\sin^2\gamma)]}{1008},$$

$$c_8 = \frac{1}{56}\left\{-14c_7 - \left[\lambda^2 + c^2\left(d\cos\gamma + \frac{1}{2}d^2\sin^2\gamma\right)\right]c_6 + \frac{c^2(d\cos\gamma + d^2\sin^2\gamma)c_4}{2} + \frac{c^2(d\cos\gamma + 4d^2\sin^2\gamma)c_2}{24} + \frac{\pi c^2 e_1^3}{32}\right\}.$$

REFERENCES

[1] H.M. Irvine, T.K. Caughey, The linear theory of free vibrations of a suspended cable, Proceedings of the Royal Society A 341 (1626) (1974) 299-315.

[2] H.M. Irvine, J.H. Griffin, On the dynamic response of a suspended cable, Earthquake Engineering and Structural Dynamics 4 (4) (1976) 389-402.

[3] G. Rega, Nonlinear vibrations of suspended cables--Part I: Modeling and analysis, Applied Mechanics Reviews 57 (6) (2004) 443-478.

[4] G. Rega, Nonlinear vibrations of suspended cables--Part II: Deterministic phenomena, Applied Mechanics Reviews 57 (6) (2004) 479-514.

[5] A. Berlioz, C. Lamarque. A non-linear model for the dynamics of an inclined cable, Journal of Sound and Vibration 279 (3) (2005) 619-639.

[6] L.H. Wang, G. Rega, Modelling and transient planar dynamics of suspended cables with moving mass, International Journal of Solids and Structures 47 (2010) 2733-2744.

[7] A. Luongo, G. Piccardo, A continuous approach to the aeroelastic stability of suspended cables in 1:2 internal resonance, Journal of Vibration and Control 14 (1-2) (2008) 135-157.

[8] P.P. Roy, Cable stayed bridge, International Journal of Science and Advanced Technology 3 (7) (2013) 52-55.

[9] M. Gu, On wind-rain induced vibration of cables of cable-stayed bridges based on quasi-steady assumption, Journal of Wind Engineering and Industrial Aerodynamics 97 (7) (2009) 381-391.

[10] A. Larsen, G.L. Larose, Dynamic wind effects on suspension and cable-stayed bridges, Journal of Sound and Vibration 334 (2015) 2-28.

[11] J.M. Caicedo, S.J. Dyke, S.J. Moon et al., Phase II benchmark control problem for seismic response of cable-stayed bridges, Journal of Structural Control 10 (2003) 137-168.

[12] S.J. Dyke, J.M. Caicedo, G. Turan et al., Phase I benchmark control problem for seismic response of cable-stayed bridges, Journal of Structural Engineering 129 (7) (2003) 857-872.

[13] Y. Pang, Seismic fragility assessment of an isolated multipylon cable-stayed bridge using shaking table tests, Advances in Civil Engineering 2017 (2017) 9514086.

[14] H.J. Kang, T.D. Guo, Y.Y. Zhao et al., Dynamic modeling and in-plane 1:1:1 internal resonance analysis of cable-stayed bridge, European Journal of Mechanics-A/Solids 62 (2017) 94-109.

[15] A.M. Abdelghaffar, M.A. Khalifa, Importance of cable vibration in dynamics of cable-stayed bridge, Journal of Engineering Mechanics 117 (11) (1991) 2571-2589.

[16] J.L. Lilien, A.P. Costa, Vibration amplitudes caused by parametric excitation of cable stayed structures, Journal of Sound and Vibration 174 (1) (1994) 69-90.

[17] C.Z. Qian, C.P. Chen, and G.W. Zhou, Nonlinear dynamical analysis for the cable excited with parametric and forced excitation, Journal of Applied Mathematics 2014 (2014) 183257.

[18] L. Chen, L. Sun, Steady-state analysis of cable with nonlinear damper via harmonic balance method for maximizing damping, Journal of Structural Engineering 143 (2) (2017) 04016172.

[19] X.Y. Su, H.J. Kang, T.D. Guo et al., Modeling and parametric analysis of in-plane free vibration of a floating cable-stayed bridge with transfer matrix method,

International Journal of Structural Stability and Dynamics, Accepted 2019. https://doi.org/10.1142/S0219455420500042

[20] X.Y. Su, H.J. Kang, J. Chen et al., Experimental study on in-plane nonlinear vibrations of the cable-stayed bridge, Nonlinear Dynamics 98 (2) 2019: 1247-1266.

[21] K. Nithesh, K.K. Shetty, P. Shenoy, Influence of cable profiles on the performance of cable stayed bridge, International Journal of Civil Engineering and Technology 9 (5) (2018): 1136-1148.

[22] S.K. Lai, Y. Xiang, C.W. Lim et al., Higher-order approximate solutions for nonlinear vibration of a constant-tension string, Journal of Sound and Vibration 317 (3-5) (2008) 440-448.

[23] A.H. Nayfeh, D.T. Mook, Nonlinear Oscillations, Wiley, New York, 1973.

All Figures in the Manuscript:

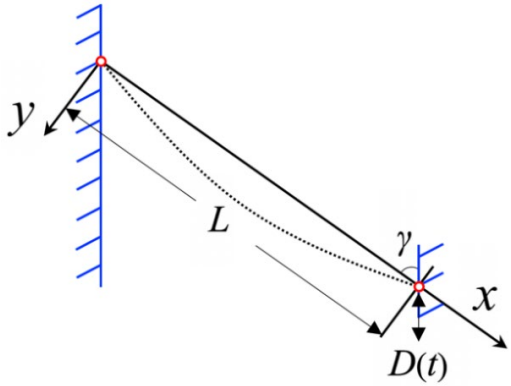

Figure 1. Schematic diagram of a cable

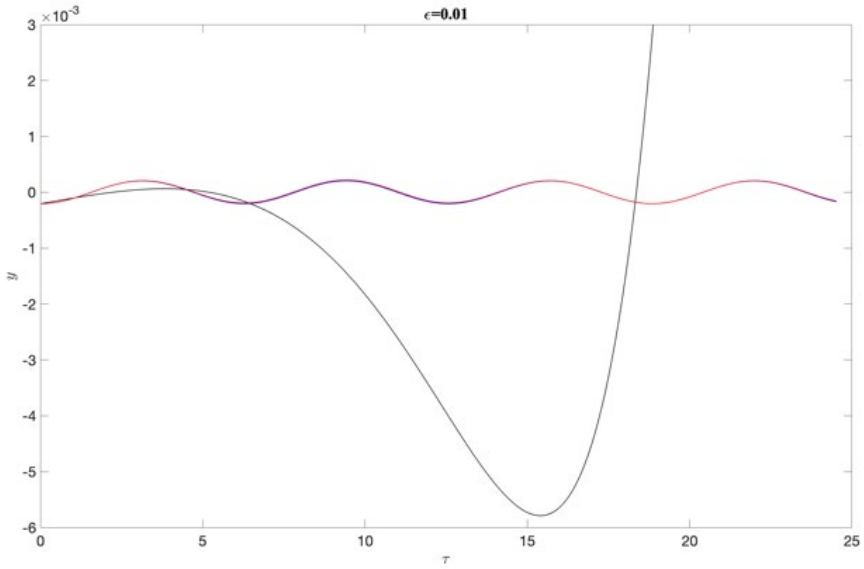

Figure 2. A comparison between the conventional perturbation method solution (black curve), the two-timing scale method solution (blue curve) and the "exact solution" (red curve).

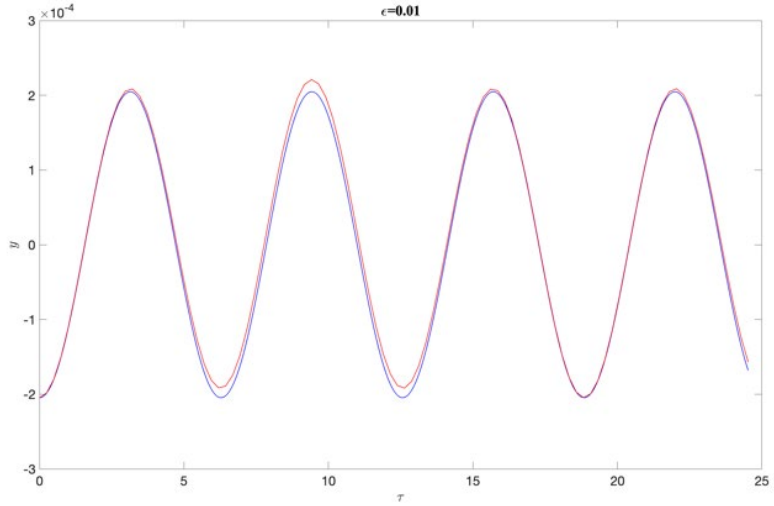

Figure 3. A comparison between the two-timing scale method solution (blue curve), and the "exact solution" (red curve).

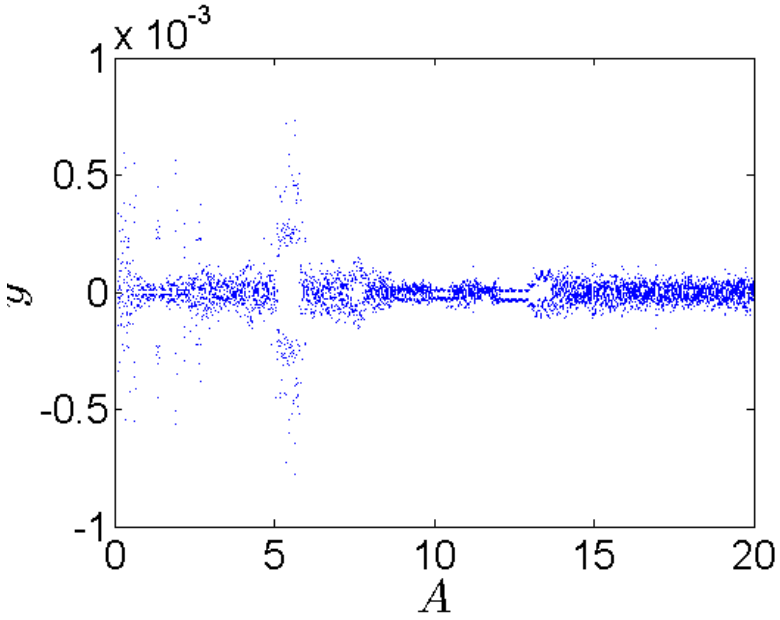

Figure 4. Bifurcation diagram for the cross-sectional area of the cable (A) and the displacement (y).

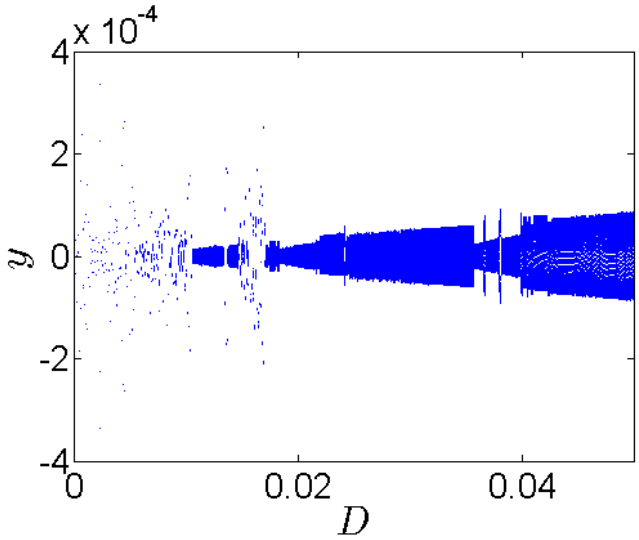

Figure 5. Bifurcation diagram for the vibration amplitude of the anchorage point (D) and the displacement (y).

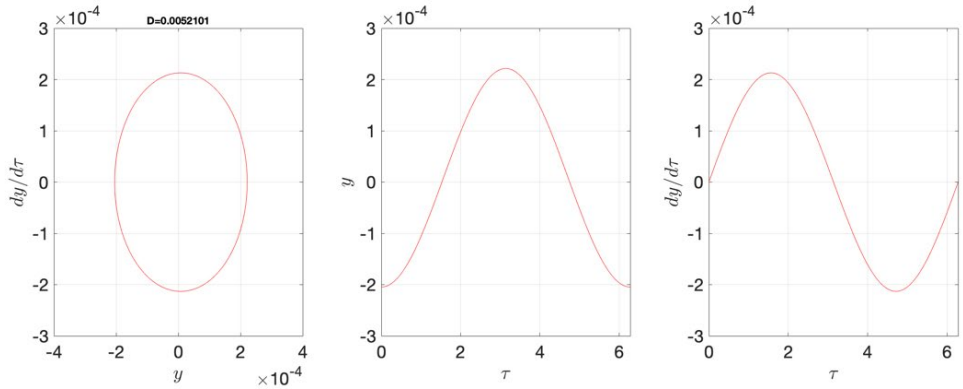

Figure 6. Phase portrait and time domain curves of the system for D = 0.0052101.

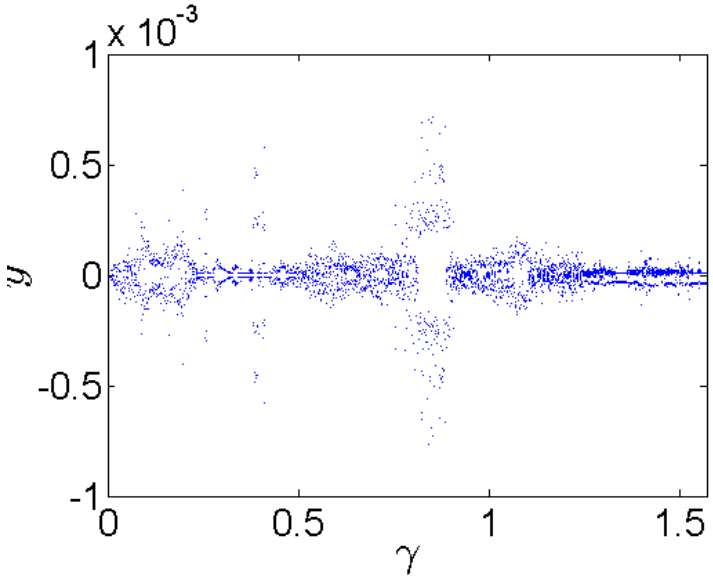

Figure 7. Bifurcation diagram for the inclination angle (γ) and the displacement (y).

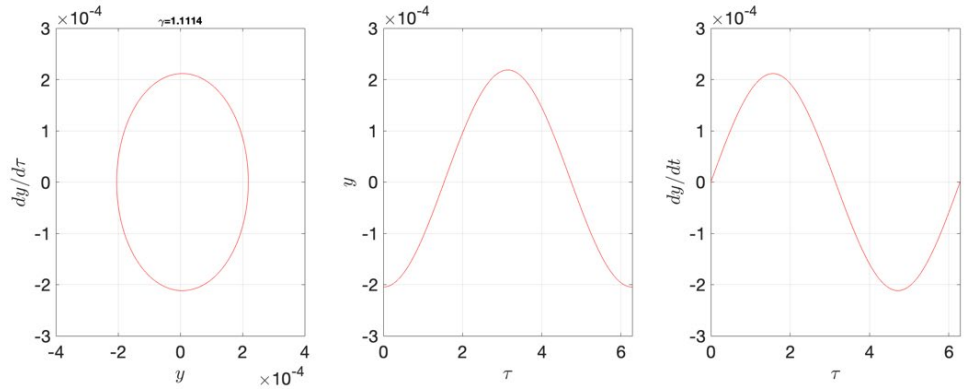

Figure 8. Phase portrait and time domain curves of the system for $\gamma = 1.1114$.

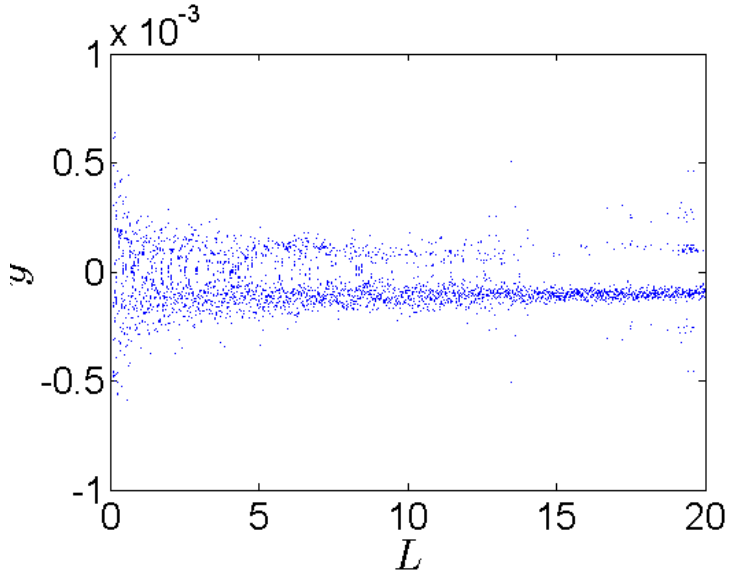

Figure 9. Bifurcation diagram for the cable length (L) and the displacement (y).

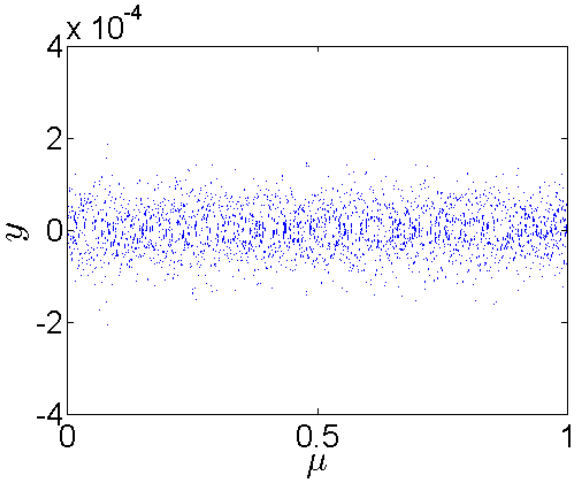

Figure 10. Bifurcation diagram for the damping effect (μ) and the displacement (y).

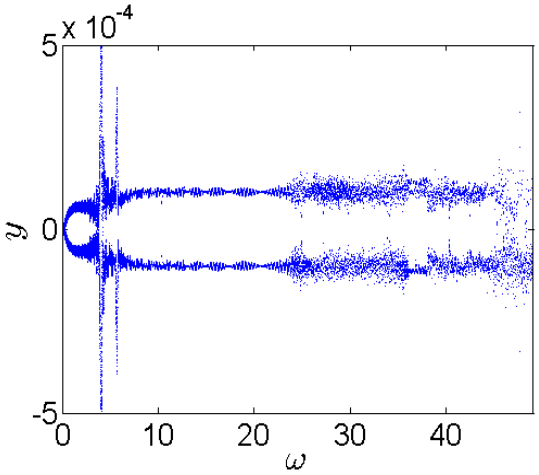

Figure 11. Bifurcation diagram for the excitation frequency (ω) and the displacement (y).

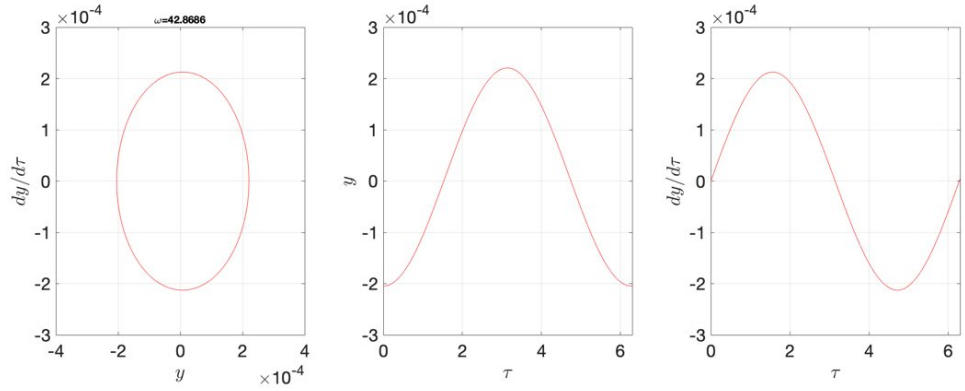

Figure 12. Phase portrait and time domain curves of the system for $\omega = 42.8686$.

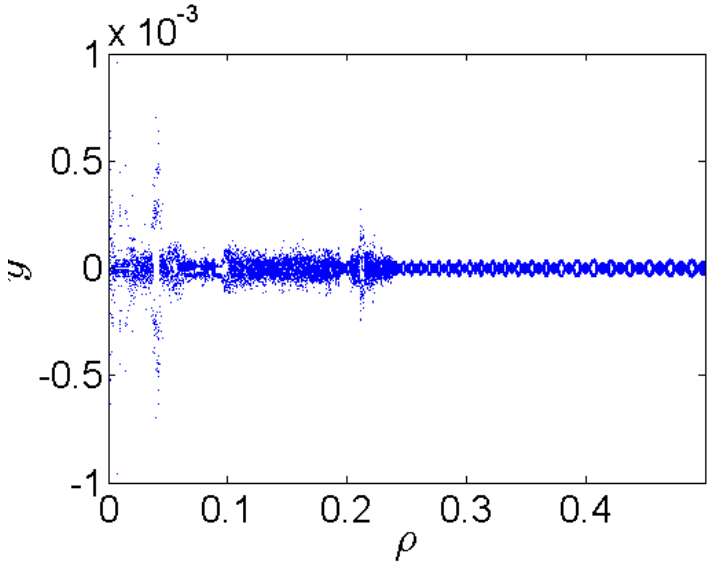

Figure 13. Bifurcation diagram for the cable density (ρ) and the displacement (y).

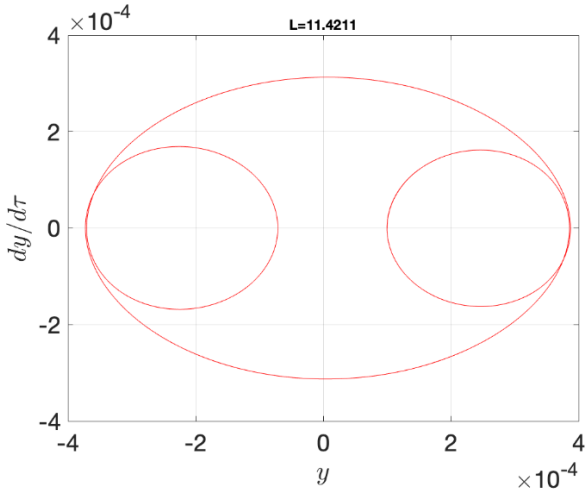

Figure 14. Phase portrait diagram for L = 11.4211 and $[a, b] = [0.0001, 0]$.

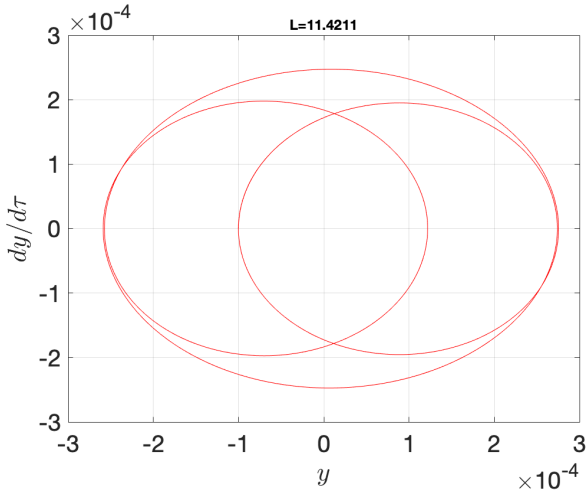

Figure 15. Phase portrait diagram for L = 11.4211 and $[a, b] = [-0.0001, 0]$.

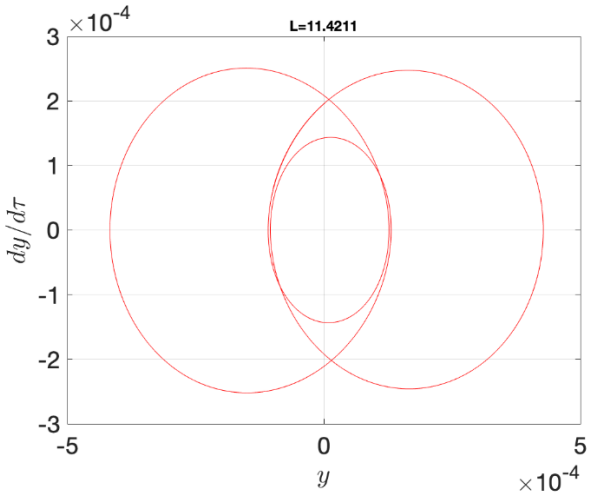

Figure 16. Phase portrait diagram for $L = 11.4211$ and $[a, b] = [-0.0001, 0.00006]$.

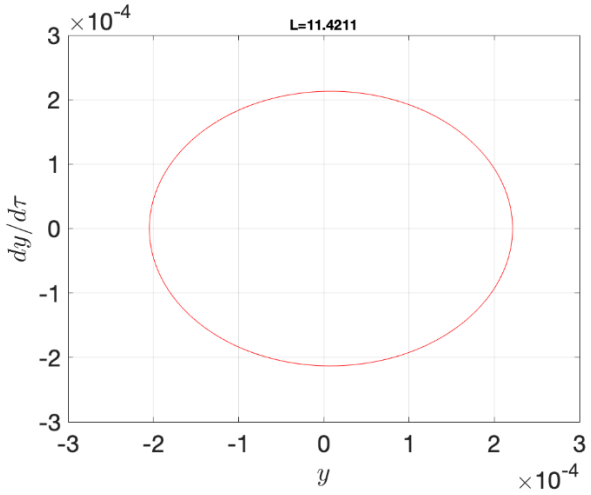

Figure 17. Phase portrait diagram for $L = 11.4211$ and $[a, b] = [-0.002046, 0]$.

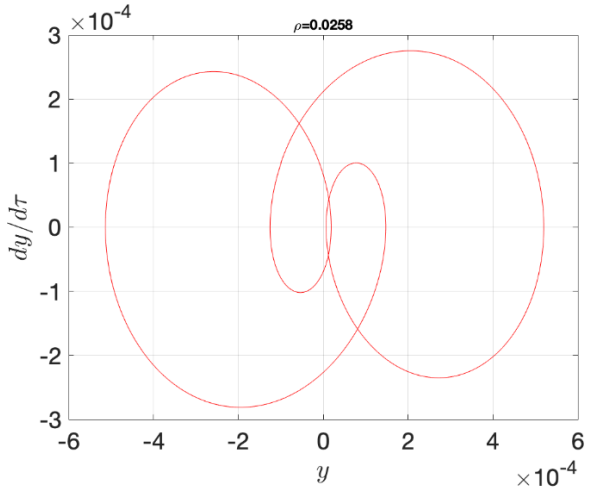

Figure 18. Phase portrait diagram for $\rho = 0.0258$ and $[a, b] = [-0.0001, 0.0001]$.

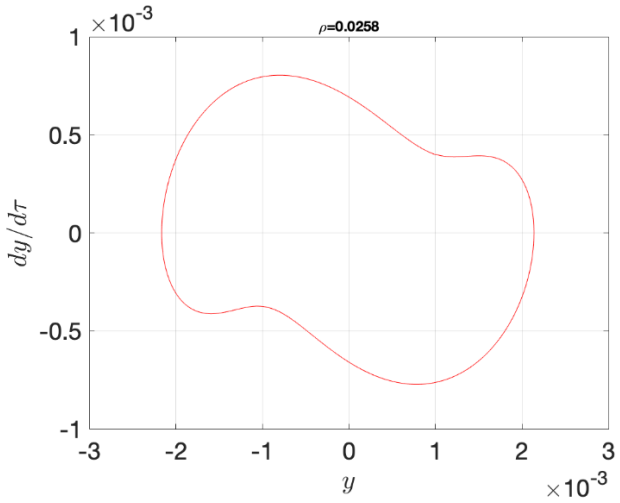

Figure 19. Phase portrait diagram for $\rho = 0.0258$ and $[a, b] = [0.001, 0.0004]$.

Table in the Manuscript:

Table 1: The geometrical and material properties of a cable [17]

Mass per unit length (W)	0.391 kg/m
Length of cable (L)	11.90 m
Sectional area (A)	7.28 mm^2
Axial tensile force (T)	1.5×10^4 N
Elastic modulus (E)	8.242×10^4 MPa
Vibration amplitude of the anchorage point (D)	5 mm
Natural frequency (ω_0)	16.3515 Hz